ISSN 2176-5480

22nd International Congress of Mechanical Engineering (COBEM 2013)
November 3-7, 2013, Ribeirão Preto, SP, Brazil

EXPERIMENTAL MEASUREMENTS OF A TURBULENT FLOW OVER A LOW HILL

Erick de Moraes Franklin
Guilherme Augusto Ayek
Faculdade de Engenharia Mecânica - UNICAMP
franklin@fem.unicamp.br
guilhermeayek@hotmail.com

Abstract. *This paper presents an experimental study on the perturbation of a fully-developed turbulent boundary layer by a two-dimensional hill. Different water flows were imposed over a hill fixed on the bottom wall of a closed conduit and the flow field was measured by PIV (Particle Image Velocimetry). Reynolds numbers based on the channel height varied between 17000 and 35000 and the regime was hydraulically smooth. The general behaviors of obtained velocities and stresses are compared to published asymptotic analyses and the surface shear stress is discussed in terms of instabilities of a granular bed. Our results show that, depending on the Reynolds number, the inner regions of the perturbed flow are not in local equilibrium and therefore the perturbation expressions based on local-equilibrium conditions must be employed with care.*

Keywords: *Turbulent boundary layer, closed conduit, perturbation, instability, hill*

1. INTRODUCTION

Turbulent boundary layers perturbed by a low hill are commonly found in nature and in industry. Some examples are air flows over hills, water flows over river dunes and closed-conduit flows over sand ripples. The latter is frequently encountered in industrial facilities, such as petroleum pipelines, dredging lines and sewer systems. The perturbation of the boundary layer introduces new scales in the problem, and the new velocity and stress distributions are of importance for many environmental and industrial applications. For example, when in the presence of sediment transport the stress distribution along the hill is an essential parameter to understand the bed instabilities.

Many studies were devoted over the last decades to the perturbation of a turbulent boundary layer by a low hill (Jackson and Hunt, 1975; Hunt et al., 1988; Belcher and Hunt, 1998), improving our knowledge on the subject. A great part of them were based on asymptotic methods, that considers small aspect ratio hills and divides the turbulent boundary layer in regions, each one with its pertinent scales. A solution is then sought for each region knowing that they must match each other.

Jackson and Hunt (1975) divided the perturbed boundary layer in two regions: (i) an inner region, close to the bed, where the time scale for the dissipation of the energy-containing eddies is much smaller than the time scale for their advection, so that this region is in local equilibrium; (ii) an outer region, far from the bed, where the time scale for the dissipation of the energy-containing eddies is much larger than the time scale for their advection, so that the flow is not in local equilibrium. In the inner region, the local-equilibrium condition allows the use of turbulent stress models. In addition, its thickness is small and the perturbations are considered driven by the pressure field of the outer region. In the outer region, a potential solution is expected at the leading order because the mean flow is almost unaffected by the shear stress perturbations. Jackson and Hunt (1975) found solutions for each region and matched them, obtaining a solution for the perturbation. Their composite solution shows that most of the perturbation occurs in the inner region and that it has an upstream shift with respect to the hill.

Hunt et al. (1988) improved the analysis of Jackson and Hunt (1975) by subdividing each region in two layers and obtained results in agreement with that of Jackson and Hunt (1975). Hunt et al. (1988) also showed that the maximum of the perturbation velocity occurs in the shear stress layer and that near the surface the relative increase of the surface stress is greater than that of velocity. In addition, they extended the analysis to three-dimensional hills.

Based on Jackson and Hunt (1975) and Hunt et al. (1988), Weng et al. (1991) computed the velocity perturbations until the second order and applied the results to forms with higher aspect ratios. The proposed expressions for the surface stresses, at the first order, are largely employed. Kroy et al. (2002a, 2002b) simplified the results of Weng et al. (1991) for the surface stress and obtained an expression containing only the dominant physical effects of the perturbation, making clear the reasons for its upstream shift. Carruthers and Hunt (1990) showed that reasonable results are obtained for higher forms, with slopes up to 0.3.

Charru and Franklin (2012) studied the evolution of the shear stress along the symmetry plane of three-dimensional isolated dunes, known as barchans. Their experimental results showed that the surface shear stress is in phase with the bedform, so that the formation of aquatic barchans cannot be understood. The absence of an upstream shift was not explained by the authors.

ISSN 2176-5480

This paper presents an experimental study on the perturbation of a fully-developed turbulent boundary layer by a two-dimensional hill. Water flows were imposed over a hill fixed on the bottom wall of a closed conduit and the flow field was measured by PIV (Particle Image Velocimetry). From the flow measurements, mean and fluctuation fields were computed. The obtained velocities and stresses are compared to published asymptotic analyses and the surface shear stress is discussed in terms of instabilities of a granular bed.

2. EXPERIMENT

The experimental device consisted of a water reservoir, a progressive pump, a flow straightener, a *5m* long transparent channel of rectangular cross section, a settling tank and a return line. The water flowed in a closed loop following the above order of description. The flow straightener was placed at the channel inlet and consisted of a divergent-convergent nozzle filled with *d=3mm* glass spheres, whose function was to homogenize the water flow profile. The channel test section was *1m* long and started at 40 hydraulic diameters (*3m*) downstream of the channel inlet. There was another *1m* long section connecting the test section exit to a settling tank and the return line. Figure 1 presents a layout of the experimental device.

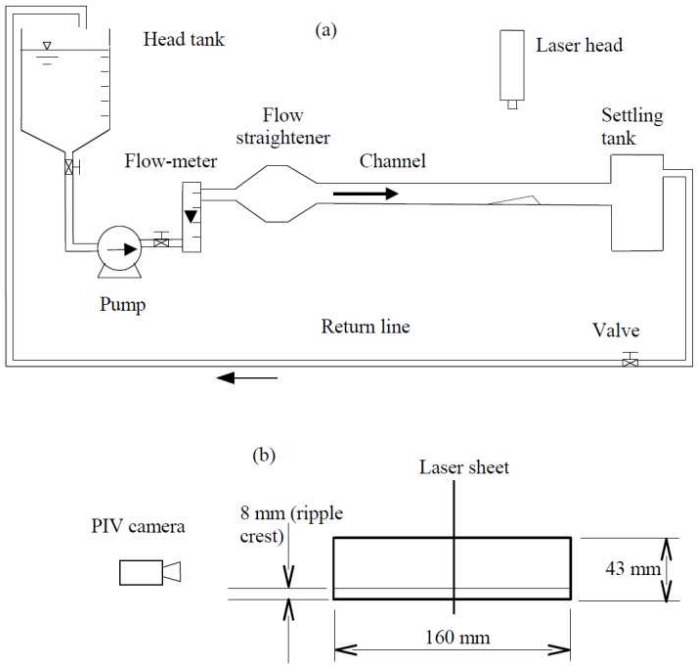

Figure 1. Experimental device: (a) side-view; (b) cross section.

The channel cross section was *160mm* wide by *50mm* high. PVC plates of *7mm* thickness were inserted in the channel, covering its entire bottom and reducing its height. City (tap) water was employed in the tests. The water flow rates were controlled by changing the excitation frequency of the pump and measured by an electromagnetic flow-meter. The flow rates varied between *5* and $10m^3/h$, corresponding to cross-section mean velocities *U* within *0.20* and *0.40m/s* and to Reynolds numbers $Re=U.2H_{eff}/\nu$ within *17000* and *35000*, where H_{eff} is the distance from the surface of the PVC plates to the top wall of the channel. The regime was hydraulically smooth in all the cases.

An *80mm* long, *8mm* height triangular shape model, with 6.9^o upwind angle and 29.7^o lee-side angle (close to the repose angle) was employed in the tests (Fig. 2). It had the same scales as the aquatic ripples and some closed-conduit dunes [8], and was fixed on a PVC plate in the test section, filling the entire channel width, to model a two-dimensional ripple.

Measurements were performed without and with the ripple in the closed conduit and were taken at the vertical symmetry plane of the channel. Particle Image Velocimetry was employed to obtain the instantaneous velocity fields of the water stream. The employed light source was a dual cavity Nd:YAG Q-Switched laser, capable to emit at *2* x *130mJ* at a *15Hz* pulse rate. The PIV images were captured by a CCD (charge coupled device) camera with a spatial resolution of *2048px* x *2048px* and acquiring pairs of images at *4Hz*. The total field employed was of *140mm x 140mm*, the

ISSN 2176-5480

employed interrogation area was of *8px* x *8px* and the computations were made with *50%* of overlap. This corresponds to *512* interrogation areas and to a spatial resolution of *0.27mm*.

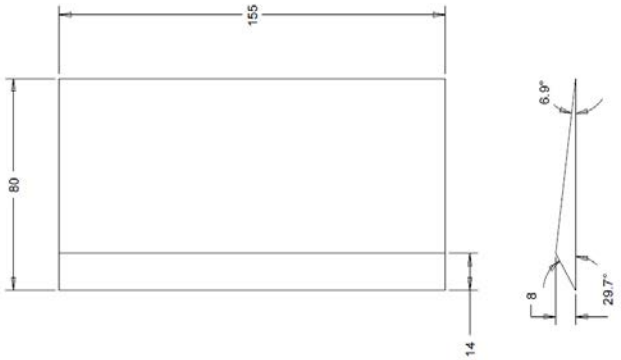

Figure 2. Model ripple of triangular shape. In this figure, the flow is downwards.

A mixture of solid particles suspended in the city water and glass spheres of *10 μm* in diameter (*S.G. = 1.05*) was employed as seeding particles. These particles required the power of the laser to be fixed at *80%* of its maximum value. Each experimental run acquired *1000* pairs of images for the tests with the ripple and *500* pair of images for the tests without the ripple. Fields of instantaneous velocity, of time-averaged velocity and of the velocity fluctuations were computed in fixed Cartesian grids by the PIV controller software (DaVis). MatLab scripts were written to post-process these fields (spatio-temporal averaged profiles, shear velocities, stresses on the ripple coordinate system, for example).

3. RESULTS AND DISCUSSION

3.1 Unperturbed flow

Initially, the water flow was measured in the absence of the ripple, corresponding then to a turbulent, unperturbed, fully-developed channel flow. This case is indicated in the following by the subscript *0*. Flow rates of *5, 5.6, 6.1, 6.8* and *7.3 m^3/h* were imposed, corresponding to cross-section mean velocities *U* of *0.20, 0.23, 0.25, 0.27* and *0.29 m/s* and to Reynolds numbers *Re* of *18000, 20000, 22000, 24000* and *26000*.

For each test, the instantaneous fields were time-averaged and the fluctuation fields (second-order moments) were computed and time-averaged. The time-averaged fields were then space-averaged in the longitudinal direction because the flow was fully developed. With this procedure, vertical profiles of the mean velocities and of second-order moments were obtained taking advantage of the spatial resolution of the PIV equipment. The measurements showed that the law of the wall and the Blasius correlation are valid for the turbulent flow in the test section and therefore can be used to estimate the unperturbed flow.

Figure 3a presents the log-normal profiles of the mean velocities for different Reynolds numbers. The abscissa is in logarithmic scale and represents the vertical distance from the channel walls (bottom or top) normalized by the viscous length, y^+. The ordinate is in linear scale and corresponds to the mean velocities normalized by the shear velocity, ${u_0}^+$. Given the logarithmic scales of y^+, the profiles for each flow rate are depicted in two parts: one from the bottom wall until the channel axis of symmetry, represented by the open symbols; and the other from the top wall until the channel axis of symmetry, represented by the filled symbols. The circles, lozenges, inverted triangles, triangles and squares correspond to $Re = 1.8 \times 10^4, 2.0 \times 10^4, 2.2 \times 10^4, 2.4 \times 10^4$ and 2.6×10^4, respectively. Figure 3a shows that the profiles follow the law of the wall, with a well defined logarithmic region. In addition, the profiles for different Reynolds numbers, for both the bottom and the top walls, are perfectly superposed.

ISSN 2176-5480

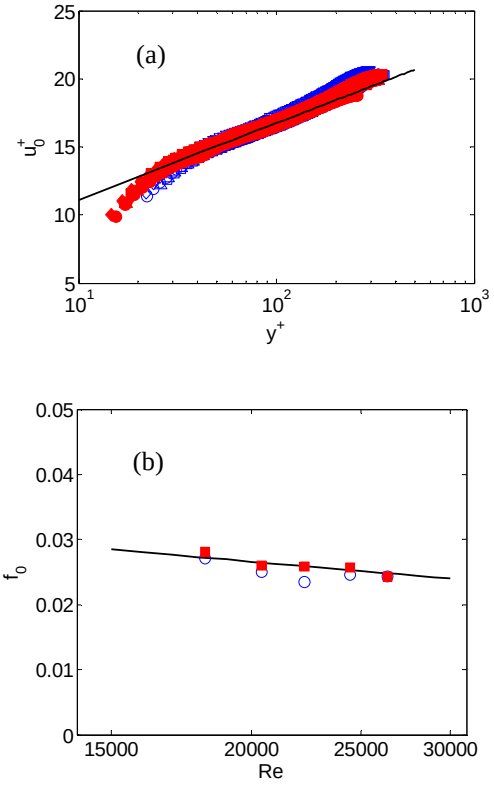

Figure 3. (a) Velocity profiles (b) Friction factor as a function of *Re.*

Figure 3b presents the friction factor f_0 as a function of the Reynolds number *Re*. The open symbols correspond to f_0 on the bottom wall, the filled symbols to f_0 on the top wall and the continuous line corresponds to the Blasius correlation for smooth walls.

3.2 Perturbed flow

Three different flow rates were employed in the tests with the ripple: *5*, *7.5* and *10* m^3/h. They correspond to *U=0.20m/s, 0.30m/s* and *0.40m/s*, to *Re=18000, 26000* and *35000*, respectively.

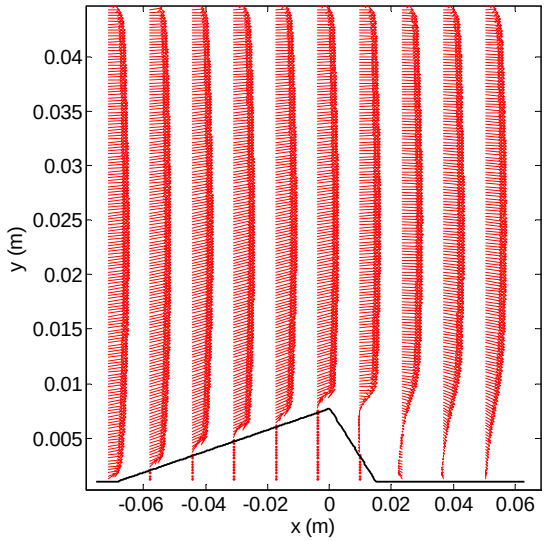

Figure 4. Some profiles of the perturbed mean velocities over the ripple. The flow is from left to right and *Re=35000*.

Figure 4 presents some mean velocity profiles $\vec{V}(y) = u(y)\vec{\imath} + v(y)\vec{\jmath}$ over the ripple. In Fig 4 and the following ones, the position $x = 0$ corresponds to the ripple crest. From this figure, we see that the perturbed flow has at least

ISSN 2176-5480

three distinct regions: (i) one far from the ripple surface where the $v \approx 0$ and the perturbation in u is small (given mainly by confinement effects); (ii) another close to the ripple surface and downstream of the crest, where a recirculation bubble exists; (iii) and another one close to the ripple surface and upstream of the crest, where v is directed upwards and the perturbation of u is stronger than far from the bed.

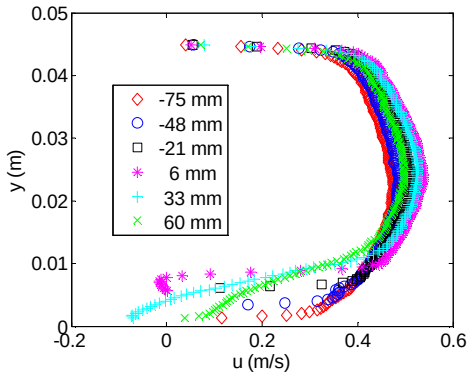

Figure 5. Longitudinal component of some mean velocity profiles *u(y)* over the ripple

Figure 5 presents the longitudinal component of some mean velocity profiles *u(y)* over the ripple. Each employed symbol corresponds to the longitudinal position indicated in the legends. This figure is suitable for an analysis of the core flow and upper wall regions, as seen next. This figure shows that the perturbation is smaller in the upper wall region and that there is a longitudinal advective acceleration of the core flow. The maximum of u does not occur at the crest ($x = 0$). This is expected because the recirculation bubble also affects the core flow.

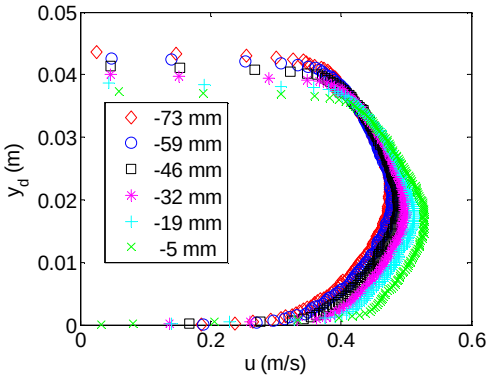

Figure 6. Longitudinal component of some mean velocity profiles $\boldsymbol{u(y_d)}$. *Re=35000.*

For the analysis of the near bed region, a vertical coordinate following the ripple surface is more suitable. The reason is that it gives as reference the solid surface where $\vec{V}(y) = 0$, necessary to the boundary-layer analysis. This vertical coordinate can be defined as

$$y_d = y - h \tag{1}$$

where $h = h(x)$ is the local height of the ripple and y_d is called displaced vertical coordinate.

Figure 6 presents the longitudinal component of some mean velocity profiles in terms of the displaced coordinate, $u(y_d)$, in the region upstream of the ripple crest. Each employed symbol corresponds to the longitudinal position indicated in the legends. In *x<0*, *u* increases as the flow approaches the ripple crest and a great part of the perturbation is confined in the lower region. The degree of acceleration of u varies with y_d, so the longitudinal position where u reaches its maximum value is not clear in Fig. 6.

ISSN 2176-5480

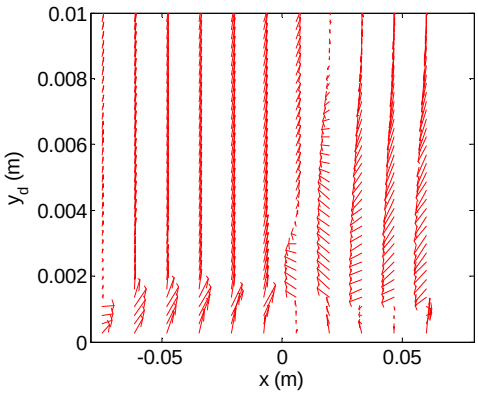

Figure 7. Some perturbation profiles of the mean velocities. *Re=35000.*

Jackson and Hunt (1975) defined the perturbation field as the difference between the flow over the ripple and that over a flat wall, in the displaced vertical coordinate. This gives:

$$\Delta\vec{V}(y_d) = \vec{V}(y_d) - \vec{V}_0(y_d) \tag{2}$$

where $\vec{V}_0(y_d)$ is the unperturbed flow. Figure 7 presents some perturbation profiles of the mean velocities along the ripple. Downstream of the crest, the flow detaches and a recirculation bubble is formed. Upstream of the crest, the perturbation is localized in the region $y_d < 2mm$. If the displaced vertical coordinate is normalized by the viscous length of the unperturbed flow, then we obtain $y_d^+ = y_d u_*/\nu < 43$. This region corresponds to the buffer and viscous layers of the unperturbed boundary layer, where the viscous shear stress is very important (Schlichting, 2000).

Concerning the formation of aquatic sand ripples, the transport of grains as a mobile bed (bed load) takes place very often in the region $y_d^+ < 20$ (Raudkivi, 1976). For this reason, the viscous shear stress on the ripple surface τ_{visc} is of interest. It may be evaluated as

$$\tau_{visc} \approx \mu\, \partial u_\theta / \partial y_{d,\theta} \tag{3}$$

where u_θ is the aligned component of the mean velocity with respect to the ripple surface and $y_{d,\theta}$ is a displaced coordinate perpendicular to the ripple surface.

In addition, the viscous stress τ_{visc} can be compared to the turbulent stresses in order to understand if the water flow is in local equilibrium in the lower layers. Figure 8 presents the evolution along the ripple of the surface viscous stress normalized by the unperturbed shear stress τ_0. Based on the unperturbed measurements (Fig. 3b), the unperturbed shear stress was evaluated from the Blasius correlation. In this figure, the continuous, dashed and dotted lines correspond to *Re=18000, 26000* and *35000* (*U=0.2m/s, 0.3m/s* and *0.4m/s*), respectively. From this figure, it seems that the maximum of the surface stress occurs upstream of the ripple crest. However, this cannot be asserted because of the relatively high noise in the data.

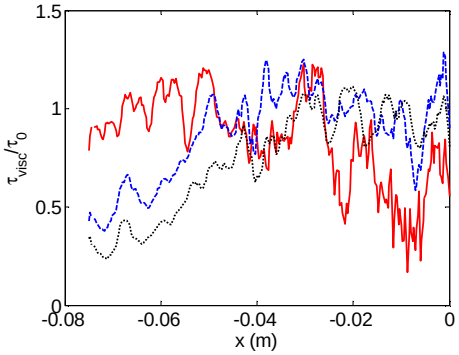

Figure 8. Normalized surface viscous stress as a function of the longitudinal position.

Turbulent stresses are of importance in the layers above the viscous layer. In the overlap and core flow layers, i.e., $y_d^+ \gtrsim 30$ (from the bed region until the channel center) and $y^+ \gtrsim 30$ (from the top wall region until the channel center), the turbulent stresses are the dominant ones. Figures 9 to 11 present the vertical profiles of the *xx*, *yy* and *xy* components of turbulent stresses in dimensionless form, respectively. In order to decrease the noise in the graphics, the profiles were

ISSN 2176-5480

averaged by a sliding window process over the closest 9 points. The values of the unperturbed shear velocity $u^2_{*,0}$ were obtained from the Blasius correlation (Fig. 3b) and $u^2_{*,0} = \tau_0/\rho$. The displaced vertical coordinate is normalized by the unperturbed viscous length. Each employed symbol corresponds to the longitudinal position indicated in the legends.

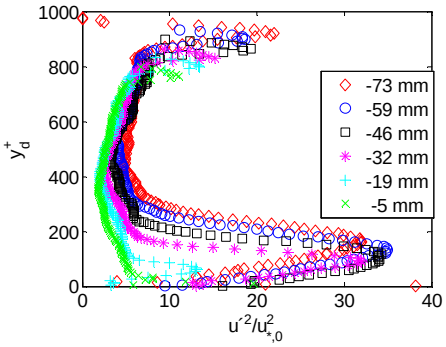

Figure 9. Some profiles of the turbulent stress *xx* component in dimensionless form upstream of the ripple crest. *Re=35000.*

The perturbations of turbulent stresses are stronger at the bottom, close to the ripple surface. In the cases of the *xx* component, $\overline{u'^2}$, and of the *yy* component, $\overline{v'^2}$, the perturbations are roughly 3 times greater near the ripple (compared to the top wall region). In the case of the *xy* component, the perturbations of $\overline{u'v'}$ are one order of magnitude greater near the ripple. At the channel center, the turbulent stresses are much smaller than near the walls. Longitudinally, we observe that the turbulent stresses vary (including near the top wall), indicating the effect of confinement on the perturbations.

The *xy* component of the turbulent stress is of particular interest. If the boundary layer is in local equilibrium, then the values of $-\overline{u'v'}$ in the overlap layer shall scale with $\tau_{visc}/\rho = u^2_*$, which in turn is expected to be a small perturbation of $\tau_0/\rho = u^2_{*,0}$. In other words, in a local-equilibrium overlap layer $-\overline{u'v'}$ has the same order of magnitude as $u^2_{*,0}$.

Figure 12 presents the vertical profiles of the *xy* component of turbulent stresses in the $y_d^+ \lesssim 300$ region, covering then the overlap layer. The turbulent stress $-\overline{u'v'}$ is normalized by the square of the unperturbed shear velocity $u^2_{*,0}$ and the displaced vertical coordinate is normalized by the unperturbed viscous length. The symbols are the same as in Fig. 11. This figure shows that, except for $x \geq -19mm$, the $-\overline{u'v'}$ profiles vary strongly across the overlap layer, reaching a peak of around 8 times $u^2_{*,0}$ (one order of magnitude higher). This is not in accordance with an overlap layer in local equilibrium.

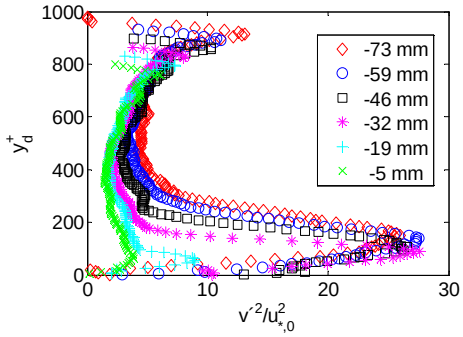

Figure 10. Some profiles of the turbulent stress *yy* component in dimensionless form upstream of the ripple crest. *Re=35000.*

ISSN 2176-5480

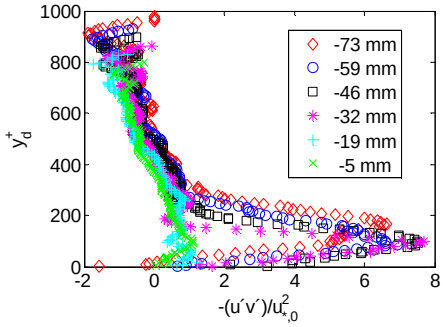

Figure 11. Some profiles of the turbulent stress *xy* component in dimensionless form upstream of the ripple crest. *Re=35000*.

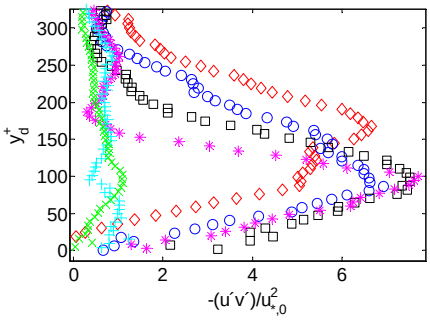

Figure 12. Some profiles of the turbulent stress *xy* component in dimensionless form upstream of the ripple crest, in the y_d^+*<300* region. *Re=35000.*

The fact that in the $x \geq -19mm$ region the $-\overline{u'v'}$ profiles are roughly constant and approximately equal to $u_{*,0}^2$ is difficult to explain. In this region, the curvature of the flow is negative and this may change the phases of *u'* and *v'*, decreasing $-\overline{u'v'}$ values. However, the most plausible explanation seems to be that local equilibrium is reached in this region, as discussed below.

Figure 13 presents the longitudinal evolution of the maximum of the *xy* turbulent stress $(-\overline{u'v'})_{max}$ (for each vertical profile) normalized by $u_{0,*}^2$, for the bottom wall region. The continuous, dashed and dotted lines correspond to *Re=18000, 26000* and *35000* (*U=0.2m/s, 0.3m/s* and *0.4m/s*), respectively. Figure 13 shows that $(-\overline{u'v'})_{max}$ reaches high values of approximately $8u_{0,*}^2$ in the *x < -0.030m* region (upstream of the ripple crest), with a peak at *x ≈ -0.04m*. Within *-0.030m < x < -0.017m*, $(-\overline{u'v'})_{max}$ decreases rapidly to $(-\overline{u'v'})_{max} \approx u_{0,*}^2$ and it remains stable at this value in the *-0.017m < x < 0.002m* region. In the *x > 0.002m* region there is the formation of a recirculating bubble and the values of $(-\overline{u'v'})_{max}$ vary strongly.

In terms of magnitude, there is a large difference between $-\overline{u'v'}$ and τ_{visc} in the *x < -0.030m* region: $\tau_{visc}/(-\overline{u'v'})_{max} = O(0.1)$. This corroborates the observations made for the $-\overline{u'v'}$ profiles (Fig. 12): the region corresponding to the overlap layer of the unperturbed flow is not in local equilibrium in the *x < -0.030m* region.

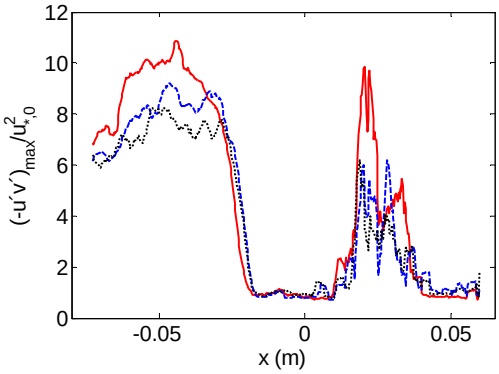

Figure 13. Maxima of the *xy* component of the normalized turbulent stress as a function of the longitudinal position *x* at the bottom wall region. The continuous, dashed and dotted lines correspond to *Re=18000, 26000* and *35000*, respectively.

ISSN 2176-5480

It seems to us that in the *-0.017m < x < 0.02m* region the flow has reached local-equilibrium conditions. The reasons for this are: (i) the $(-\overline{u'v'})_{max}$ decrease in the *-0.030m < x < -0.017m* region is gradual, although fast, with roughly *50* data points in this region; (ii) the stable value reached within the *-0.017m < x < 0.002m* region is of the same order of magnitude as both $u_{0,*}^2$ and of τ_{visc}.

4. CONCLUSIONS

This paper investigated experimentally the perturbation of a fully-developed turbulent boundary layer by a two-dimensional hill. In the experiments, turbulent water flows were perturbed by a ripple of triangular shape fixed on the bottom wall of a closed conduit and the flow was measured by PIV. The employed Reynolds numbers were moderate, *17000<Re<35000* and the regime was hydraulically smooth. For moderate Reynolds numbers, the results showed that:

- The maximum of the turbulent shear stress on the ripple surface occurs upstream of the ripple crest. For the triangular ripple, it was found to occur at 5*0%* of the ripple length *L* (measured from the crest). This shift is necessary to explain the instabilities giving rise to aquatic ripples in the hydraulic smooth regime.
- In the *x/L<40%* region (measured from the crest), the turbulent stresses are much higher than both the surface viscous stresses (local) and the square of the unperturbed shear velocity. In addition, the $-\overline{u'v'}$ vertical profiles vary strongly along the layer corresponding to the unperturbed overlap layer. These characteristics indicate that the flow is not in local equilibrium in this region.
- In the *20%<x/L<0%* region (measured from the crest), the maxima of the turbulent stresses are of the same order of magnitude as both the viscous stresses and the square of the unperturbed shear velocity. In addition, the $-\overline{u'v'}$ vertical profiles are roughly constant in the layer corresponding to the overlap layer. Based on these characteristics, it seems that the flow has reached local equilibrium in this region.

In summary, the lower layers of hydraulically-smooth turbulent flows perturbed by a low hill are not necessarily in local-equilibrium conditions. In the $O(Re) = 10^4$ case, experiments showed that over roughly *50%* of the ripple length the lower layers are not in local equilibrium. For this reason, asymptotic expressions for the boundary-layer perturbation based on local-equilibrium conditions must be employed with care whenever $Re<O(10^5)$.

5. ACKNOWLEDGEMENTS

The authors are grateful to Petrobras S.A. (contract number 0050.0045763.08.4). Erick M. Franklin is grateful to FAEPEX/UNICAMP (conv. 519.292, project 1435/12) and to FAPESP (contract number 2012/19562-6).

6. REFERENCES

Belcher, S.E. and Hunt, J.C.R., 1998. “Turbulent flow over hills and waves”, *Ann. Rev. Fluid Mech.* Vol. 30, pp. 507-538.

Carruthers, D. J. and Hunt, J. C. R., 1990. “Fluid mechanics of airflows over hills: turbulence, fluxes, and waves in the boundary layer”, *Atmospheric Processes over Complex Terrain.* Vol. 23, pp. 83-108.

Charru, F. and Franklin, E. M., 2012. “Subaqueous barchan dunes in turbulent shear flow. Part 2: Fluid flow”, *J. Fluid Mech.* Vol. 694, pp. 131-154.

Franklin, E.M., 2010. “Initial instabilities of a granular bed sheared by a turbulent liquid flow: length-scale determination”, *J. Braz. Soc. Mech. Sci. Eng.* Vol. 32, pp. 460-467.

Hunt, J.C.R., Leibovich, S. and Richards, K., 1988. “Turbulent shear flows over low Hills”, *Quart. J. R. Met. Soc.* Vol. 114, pp. 1435 – 1470.

Jackson, P.S. and Hunt, J.C.R, 1975. “Turbulent wind flow over a low hill”, *Quart. J. R. Met. Soc.* Vol. 101, pp. 929 – 955.

Kroy, K., Sauermann, G. and Herrmann, H. J., 2002a. “Minimal model for aeolian sand dunes”, *Phys. Rev. E.* Vol. 66 (031302).

Kroy, K., Sauermann, G. and Herrmann, H. J., 2002b. “Minimal model for sand dunes”, *Phys. Rev. Lett.* Vol. 88 (054301).

Raudkivi, A.J., 1976. *Loose boundary hydraulics*, Pergamon.

Schlichting, H., 2000. *Boundary-layer theory*, Springer.

Weng, W.S., Hunt, J.C.R., Carruthers, D.J., Warren, A., Wiggs, G.F.S., Livingstone, I. and Castro, I., 1991. “Air flow and sand transport over sand-dunes”, *Acta Mechanica.* pp. 1-21, 1991.

ISSN 2176-5480

7. RESPONSIBILITY NOTICE

The authors are the only responsible for the printed material included in this paper.